The effects of LXR agonist T0901317 and LXR antagonist GSK2033 on morphogenesis and lipid properties in full thickness skin models

Helder, R.W.J.; Boiten, W.A.; Dijk, R. van; Gooris, G.S.; El Ghalbzouri, A.; Bouwstra, J.A.

BBA - Molecular and Cell Biology of Lipids 1865 (2020) 158546

Contents lists available at ScienceDirect

BBA - Molecular and Cell Biology of Lipids

journal homepage: www.elsevier.com/locate/bbalip

The effects of LXR agonist T0901317 and LXR antagonist GSK2033 on morphogenesis and lipid properties in full thickness skin models

Richard W.J. Helder[a], Walter A. Boiten[a], Rianne van Dijk[a], Gerrit S. Gooris[a], Abdoelwaheb El Ghalbzouri[b], Joke A. Bouwstra[a,*]

[a] Division of Biotherapeutics, LACDR, Leiden University, Leiden, the Netherlands
[b] Department of Dermatology, LUMC, Leiden, the Netherlands

ARTICLE INFO

Keywords:
Skin
Ceramides
Free fatty acids
Nuclear receptors/LXR
Stearoyl-CoA desaturase
Monounsaturated
Atopic dermatitis

ABSTRACT

Full thickness models (FTMs) are 3D-cultured human skin models that mimic many aspects of native human skin (NHS). However, their stratum corneum (SC) lipid composition differs from NHS causing a reduced skin barrier. The most pronounced differences in lipid composition are a reduction in lipid chain length and increased monounsaturated lipids. The liver-X-receptor (LXR) activates the monounsaturated lipid synthesis *via* stearoyl-CoA desaturase-1 (SCD-1). Therefore, the aim was to improve the SC lipid synthesis of FTMs by LXR deactivation. This was achieved by supplementing culture medium with LXR antagonist GSK2033. LXR agonist T0901317 was added for comparison. Subsequently, epidermal morphogenesis, lipid composition, lipid organization and the barrier functionality of these FTMs were assessed. We demonstrate that LXR deactivation resulted in a lipid composition with increased overall chain lengths and reduced levels of monounsaturation, whereas LXR activation increased the amount of monounsaturated lipids and led to a reduction in the overall chain length. However, these changes did not affect the barrier functionality. In conclusion, LXR deactivation led to the development of FTMs with improved lipid properties, which mimic the lipid composition of NHS more closely. These novel findings may contribute to design interventions to normalize SC lipid composition of atopic dermatitis patients.

1. Introduction

Human skin equivalents (HSEs) are 3D-cultured skin models that mimic the properties of NHS in many aspects and can therefore serve as a model to unravel biological processes in healthy and diseased skin [1]. However, one of the most important drawbacks of HSEs is an impaired skin barrier function. This limits its use to test pharmaceutical ingredients for penetration studies as an alternative to animal studies [2,3]. As the stratum corneum (SC) lipids play a crucial role in the barrier function, there in an urgent need for HSEs that harbor the lipid composition mimicking that of NHS more closely.

The main lipid classes in SC are cholesterol (CHOL), free fatty acids (FFAs) and ceramides (CERs). From these lipids, the CERs are the most complex. Many different subclasses of CERs have been identified and each subclass has a broad chain length distribution [4–7]. Together, these lipids assemble in two crystalline lamellar phases, the long periodicity phase (LPP) with a repeat distance of 13 nm and the short periodicity phase (SPP) with a repeat distance of 6 nm [8]. Within the lipid lamellae, the lipids adopt a very dense (orthorhombic), dense (hexagonal), or loose (liquid) packing. This lipid arrangement is referred to as the lateral packing (more detailed information regarding the lipid organization is provided in Supplementary Fig. S1).

Previous studies have demonstrated the importance of supplements to the medium for developing skin cultures. As an example, the supplementation with vitamin C and FFAs improved the lipid properties of the HSE to a great extent [9,10]. Although much improvement is made, important differences still remain [3]. The most pronounced differences are i) an altered CER subclass distribution, ii) a reduced chain length of the CERs and FFAs [3], iii) an increased CER/FFA ratio, and iv) an increased level of monounsaturated CERs (muCERs) and

Abbreviations: HSE, human skin equivalent; FTM, full thickness models; NHS, native human skin; SC, stratum corneum; CER, ceramide; saCER, saturated ceramide; muCER, monounsaturated ceramide; FFA, free fatty acid; saFFA, saturated free fatty acid; muFFA, monounsaturated free fatty acid; LPP, long periodicity phase; SPP, short periodicity phase; SCD-1, stearoyl-CoA desaturase 1; LXR, liver-X-receptor

* Corresponding author at: Einsteinweg 55, 2333 CC Leiden, Zuid-Holland, the Netherlands.
E-mail addresses: r.w.j.helder@lacdr.leidenuniv.nl (R.W.J. Helder), w.a.boiten2@lacdr.leidenuniv.nl (W.A. Boiten), r.van.dijk@vu.nl (R. van Dijk), g.gooris@lacdr.leidenuniv.nl (G.S. Gooris), a.ghalbzouri@lumc.nl (A. El Ghalbzouri), bouwstra@lacdr.leidenuniv.nl (J.A. Bouwstra).

https://doi.org/10.1016/j.bbalip.2019.158546
Received 30 June 2019; Received in revised form 21 September 2019; Accepted 25 September 2019
Available online 31 October 2019

monounsaturated FFAs (muFFAs) [11]. All these changes are known to reduce the skin barrier [12–14].

One of the key regulators of the epidermal lipid synthesis is the liver-X-receptor (LXR). The function of LXR is to remove excess of cholesterol *via* ABCA1 receptor. LXR also stimulates the lipid synthesis and activates genes such sterol regulatory element binding protein 1c (SREBP-1c) and stearoyl-CoA desaturase-1 (SCD-1) [15,16]. SCD-1 is drastically upregulated in HSEs during culture [17]. Therefore, we hypothesize that deactivation of LXR may initiate SCD-1 down-regulation and subsequently reduce the fraction of muCERs and muFFAs. These changes may improve the SC lipid properties drastically.

Our aim was to examine if deactivation of LXR would reduce the fraction of monounsaturated lipids in SC of our in-house developed HSE: the full thickness model (FTM). Importantly, in this study, the aim was to optimize the FTM lipid composition, rather than the full elucidation of the liver-X-receptor. To this end, FTMs were supplemented with LXR antagonist GSK2033 during culture and compared to FTMs supplemented with LXR agonist T0901317. All FTMs were assessed on i) epidermal morphogenesis, ii) SCD-1 expression and iii) CER and FFA profiling using state-of-the-art liquid chromatography coupled to mass spectrometry (LC-MS) and iv) the subsequent changes in lipid organization.

The findings in this study demonstrate that the LXR antagonist GSK2033 reduces the fraction of monounsaturated lipids and increases the chain length of FFA and CERs resulting in a slight improvement in the lipid organization. This finding can be a valuable approach for the new generation of FTMs that resemble NHS more closely.

2. Materials and methods

2.1. Primary cell isolation and monolayer cultures

Upon arrival, the human skin was cleaned with Demi H_2O and 70% ethanol after most of the fat tissue was removed. The skin was stretched on a piece of Styrofoam and dermatomed to a thickness of 400 μm. Then the skin was placed overnight in 2.4 U/mL dispase II (Roche, Almere, The Netherlands). The next day, the epidermis was separated from the dermis and used for the isolation of keratinocytes and fibroblasts as described in details elsewhere [3].

2.2. Generation of the full thickness models

The LXR agonist T091317 and LXR antagonist GSK2033 were purchased from Sigma-Aldrich (Zwijndrecht, the Netherlands). The amount of added dimethylsulfoxide was 0.05% of the total medium (v/v). LXR agonist T0901317 (500 nM) and LXR antagonist GSK2033 (500 nM) were dissolved in this volume of dimethylsulfoxide. The dermal compartment was prepared as described previously [3,18]. Isolated rat-tail collagen was used in the dermal matrix as described previously [19]. In each filter insert (Corning Transwell cell culture inserts, membrane diameter 24 mm, pore size 3 μm; Corning Life Sciences, The Netherlands) 1 mL of a 4 mg/mL collagen solution prepared in acetic acid (0.01% v/v) was used to generate a collagen layer. This layer was polymerized at 37 °C during 30 min. Subsequently, 3 mL collagen solution was mixed with fibroblasts (4.0×10^4 cells/mL collagen) and added on top of the first layer and subsequently polymerized. The dermal compartment was cultured for 7 days as described previously [3]. After this period, 2.5×10^5 keratinocytes were seeded onto each dermal compartment and cultured for 4 days at submerged conditions. Then FTMs were lifted to the air-liquid interface and cultured for a period of 14–17 days [9,18]. During this period, DMSO, LXR agonist T0901317, or LXR antagonist GSK2033 were supplemented to the culture medium. The effect of DMSO was included in the analysis, but led to no significant change in all parameters analyzed compared to $FTM_{CONTROL}$ (data not shown).

All studies were performed in triplicate using keratinocytes and fibroblasts from three different donors. After 14–17 days at the air-liquid interface period, FTMs were harvested and the following analysis were performed: quantitative polymerase chain reaction (qPCR), immunohistochemistry, LC-MS, small angle X-ray diffraction, and Fourier transformed infrared spectroscopy. The qPCR and immunohistochemistry analysis are described in the Supplementary Material and Methods.

2.3. Stratum corneum isolation

For the LC-MS, FTIR, and SAXD measurements, isolated SC was used. The SC was isolated by placing dermatomed skin (in case of NHS) or the FTMs on a cotton pad soaked in an 0.1% (w/v) trypsin (Sigma Aldrich Chemie, Zwijndrecht, The Netherlands) in PBS solution. PBS composition was 0.1 M and consisted of NaCl (8.13 g), NA_2HPO_4 (2.87 g), $KHPO_4$ (0.20 g) and KCl (0.19 g) in 1 L of MilliQ water and set to a pH of 7.4. After incubation at 4 °C overnight, the next day the skin was placed at 37 °C for 1 h. After SC separation, SC was washed with 0.1% (w/v) trypsin inhibitor (Sigma Aldrich Chemie, Zwijndrecht, The Netherlands) in PBS and subsequently washed twice with MilliQ. After washing the SC was air-dried and stored under argon in the dark until it was used.

2.4. Liquid chromatography - mass spectrometry (LC-MS)

2.4.1. Lipid extraction

Lipid extraction of SC was performed using an adapted Bligh and dyer extraction procedure as described previously [20]. After extraction, samples were stored under argon at 4 °C until CER and FFA analysis was performed. SC of NHS originated from 3 different skin donors (female, age 18–26). After storage, samples were prepared and processed according to CER or FFA analysis.

2.4.2. CER analysis

Samples were evaporated under a gentle stream of nitrogen at 40 °C and reconstituted in 95:$2_{1/2}$:$2_{1/2}$ (v/v/v) heptane:chloroform:methanol to a concentration of 0.3 mg/mL. After reconstitution, deuterated internal injection standard CER[NS] (C24deuterated; C18 protonated, Evonik Industries, Essen, Germany), was added. Subsequently, 5 μL of this sample was injected into the UPLC. The UPLC-MS setup consisted of an Acquity UPLC H-class (waters, Milford, MA, USA) coupled to an XEVO TQ-S mass spectrometer (waters, Milford, MA, USA) with an atmospheric pressure chemical ionization (APCI) chamber. Detection occurred in positive ion mode measuring full scan *m/z* between 350 and 1200 atmospheric mass units (amu). Separation of CERs was performed on a PVA-Sil column (5 μm particles size, 100 × 2.1 mm i.d., YMC, Kyoto, Japan) as described in detail before [20]. Data analysis was performed by Waters Masslynx 4.1 and area under the curve (AUC) was used for the detection of the CER species. 16 CER subclasses were analyzed. The CER class containing [N] non-hydroxy and [A] α-hydroxy are referred to as CER[non-EO]. The CER class containing the linoleic acid esterified to an ω-hydroxy are referred to as CER[EO]. The CER class containing the ω-hydroxy was referred to as CER[O]. The abbreviation of the subclasses are further explained in Supplementary Fig. S2 and referred to as introduced by Motta [21].

AUCs were corrected according to the processing method described elsewhere [20]. Some additions were made for the overlap caused by the ^{13}C isotope from the muCER to the saCER peak. This was also performed for overlap in CER[EO] and CER[O] classes. After data corrections, areas were converted to nmol and plotted in absolute values (nmol/mg SC) or CER mol (%).

2.4.3. FFA analysis

Samples were evaporated under a gentle stream of nitrogen and reconstituted in isopropanol to a concentration of 0.75 mg/mL. After adding the deuterated C24 ($C_{24}D_{47}$) internal injection standard

purchased at Sigma-Aldrich (Zwijndrecht, The Netherlands), 2 µl was injected into a UPLC. UPLC-MS setup consisted of a Waters Acquity UPLC H-class system (Waters, Milford, MA, USA) coupled to a XEVO TQ-S mass spectrometer (waters, Milford, MA, USA) connected to an atmospheric pressure chemical ionization (APCI) chamber (probe temperature: 425 °C, discharge current 3 µA). Detection occurred in negative ion mode measuring full scan *m/z* between 200 and 550 amu. FFAs were separated using a Purospher Star LiChroCART reverse phase column (3 µm particle size, 55 × 2 mm i.d., Merck, Darmstadt, Germany) between 0 and 6 min with a flow rate of 0.5 mL/min. The gradient started at acetonitrile/water/chloroform/acetic acid (90:10:2:0.005(v/v/v/v)) and shifted to methanol/heptane/chloroform/acetic acid (90:10:2:0.005). Data analysis was performed by Waters Masslynx 4.1 and the area under the curve (AUC) was calculated. FFA analysis included the following: monounsaturated FFA: (C20:1, C22:1, and C24:1) and saturated FFAs: (C20, C22, C23, C24, C25, C26, C28, and C30). As chloroform was manufacturer contaminated with FFA C16 and C18, these FFA could not be determined accurately and were therefore excluded in the analysis.

Subsequently the AUCs were corrected for the internal injection standard ($C_{24}D_{47}$) and corrected for response using FFA standards calibration curves for: C20:0, C20:1, C22:0, C22:1, C23:0, C24:0, C24:1, C25:0 C26:0, C28:0, and C30:0 (Sigma-Aldrich, Zwijndrecht, The Netherlands).

2.5. Small angle X-ray diffraction (SAXD) analysis

SAXD measurements were performed at the European Synchrotron Radiation Facility (ESRF, Grenoble, France) at station BM26B. The detailed analysis of the samples and settings is described elsewhere [12]. Isolated SC sheets were incubated for 24 h in a humidity chamber at room temperature using 27% NaBr solution (w/v) prior to measurement. Calibration of the detector was performed by using AgBH and cholesterol. Measurement was performed in 2 × 90 s and the two images were merged during sample processing. Sample distance was 2.1 m from the pilatus1M detector. One-dimensional profiles were obtained by converting the 2D detector image from Cartesian (x,y) to polar (r,θ) coordinates by integrating over θ. In case of a lamellar phase the diffraction pattern is characterized by a series of peaks at equidistant position and from the positions of these peaks the repeat distance (d) is calculated by $d = 2n\pi/q$, in which the scattering vector $q = 4\pi \sin\theta/\lambda$, where θ is the scattering angle and λ (= 0.1033 nm) is the wavelength of the X-rays.

2.6. Fourier transformed infrared spectroscopy (FTIR) analysis

FTIR measurements were performed on a Varian 670-IR spectrometer (Varian Inc., Santa Clara, CA) equipped with a broad band Mercury-Cadmium-Telluride (MCT) detector. Details of the method is described elsewhere [22]. Prior to a FTIR measurement, SC was hydrated using deuterated water in a humidity chamber for a period of 24 h. Subsequently, the SC was placed between two AgBr windows. Samples were heated from 0 to 40 °C with a gradual temperature increase of 0.25 °C/min. Spectra were collected at a resolution of 2 cm^{-1}. From the FTIR spectra, the rocking (710–740 cm^{-1}) vibrations were analyzed using the Varian resolutions pro 4.1 software.

2.7. Trans epidermal water loss (TEWL)

TEWL was measured using the isolated SC of NHS and FTMs. The SC was placed on a polycarbonate filter (Diachema, Munich, Germany) and mounted in a Permegear inline diffusion cell (Bethlehem, PA, USA). The donor compartment was empty and the acceptor compartment was filled with MilliQ water to hydrate the sample. After 15 min hydration, the TEWL was measured by an evaporimeter (Aqua Flux AF200, Biox Systems Ltd., London, UK) connected to a modified nozzle to close the donor compartment. Measurements were performed each 10 s for a period of 30 min. In the graph the average between 25 and 30 min was plotted for the samples relative to the $FTM_{CONTROL}$.

2.8. Statistical analysis

Statistical analysis was performed using Graphpad 7. A non-paired One-way ANOVA with a Holm-Sidaq posttest was used to determine significance between the FTMs and the $FTM_{CONTROL}$. Significant differences are indicated by * for $p < 0.05$, ** for $p < 0.01$, and *** for $p < 0.001$. NHS from 3 different donors was compared to the $FTM_{CONTROL}$ with an unpaired *t*-test.

3. Results

3.1. Deactivation of LXR alters the expression of lipogenic and lipid processing genes

To determine whether the LXR antagonist and agonist were delivered into the epidermal compartment of the FTMs, gene expression analysis was performed of downstream targets *ABCA1* and *ABCG1* (Fig. 1a + b).

Both genes were significantly downregulated in FTMs supplemented with GSK2033 ($FTM_{ANTAGONIST}$) and significantly upregulated in FTMs

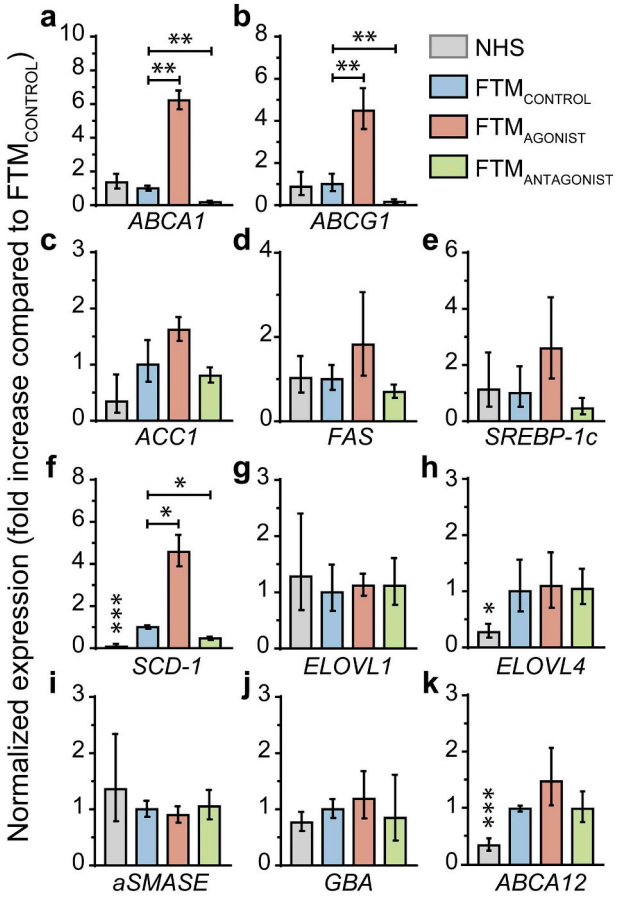

Fig. 1. LXR (de)activation affects some lipid synthesis and lipid processing genes. Genes of downstream targets: (a) *ABCA1*, (b) *ABCG1*, lipogenic genes: (c) *ACC1*, (d) *FAS*, (e) *SREBP-1c* and lipid processing enzymes (f) *SCD-1*, (g) *ELOVL1*, (h) *ELOVL4*, and late processing genes: (i) *aSMASE*, (j) *GBA*, (k) *ABCA12*. The data was normalized to the $FTM_{CONTROL}$. Statistics was applied to FTM conditions in an unpaired one-way ANOVA followed by a post Holm-Sidaq test. NHS was compared to the $FTM_{CONTROL}$ with an unpaired *t*-test. Data (n = 3) is presented as mean ± SD ($p < 0.05$ = *, $p < 0.01$ = **, $p < 0.001$ = ***).

supplemented with T0901317 ($FTM_{AGONIST}$) when compared to $FTM_{CONTROL}$ (no supplementation). This confirmed a successful epidermal targeting of LXR. Next, the effect of LXR on several lipid biosynthesis enzymes was examined, by performing gene expression analyses on the lipogenic genes *ACC1*, *FAS* and, *SREBP-1c* (Fig. 1c–e). While no significant differences were observed for the $FTM_{AGONIST}$ and $FTM_{ANTAGONIST}$, it was observed that *ACC1*, *FAS*, and *SREBP-1c* were slightly increased upon LXR activation and reduced upon LXR deactivation. Next, expression of *SCD-1* (lipid monounsaturation) was investigated (Fig. 1f). *SCD-1* showed a significant higher expression in $FTM_{CONTROL}$ compared to NHS. In $FTM_{ANTAGONIST}$, *SCD-1* expression was significantly reduced, whereas it was significantly increased in $FTM_{AGONIST}$. To study expression of the elongating enzymes, the *ELOVL1*, and *ELOVL4* gene were investigated (Fig. 1g+h). No differences in gene expression of *ELOVL1* were observed between NHS and FTMs. However, *ELOVL4* expression was significant higher in FTMs compared to NHS but no differences were observed between the various FTM conditions. Finally, late processing enzymes *GBA*, *aSMASE*, and *ABCA12* were investigated (Fig. 1i–k). No differences in expression were observed between the various FTMs, except for the *ABCA12* expression which was reduced in NHS when compared to FTMs.

3.2. (De)activation of LXR affects cell proliferation and the differentiation program

To determine the role of LXR on epidermal homeostasis, expression markers for proliferation and differentiation were investigated by immunohistochemistry and immunofluorescence (Fig. 2). The proliferation index (ki67) of the $FTM_{CONTROL}$ (15.8%) showed a significant increase ($p = 0.05$) in cell proliferation compared to NHS (12.0%). This was further increased in the $FTM_{ANTAGONIST}$ (22.1%) ($p = 0.02$), while $FTM_{AGONIST}$ showed a significant reduction (9.9%) ($p = 0.03$) in cell proliferation. Next, the early (Keratin 10 (K10)) and late (loricrin) differentiation markers were examined. K10 was expressed in the suprabasal epidermal cell layers irrespective the conditions tested, indicating normal execution of the early differentiation program.

In $FTM_{CONTROL}$ and $FTM_{AGONIST}$, loricrin stained positive in 2–3 cell layers of the stratum granulosum. Loricrin was reduced in $FTM_{ANTAGONIST}$ to 1–2 cell layers at the stratum granulosum-SC interface, more closely mimicking expression of loricrin of NHS. Finally, SCD-1 protein expression was investigated. In NHS, SCD-1 was only present in the basal layer of the epidermis. Whereas in $FTM_{CONTROL}$, SCD-1 expression was increased in the basal layer and also present in most of the suprabasal layers. In $FTM_{AGONIST}$, SCD-1 expression was even further increased, while in $FTM_{ANTAGONIST}$, a strong reduction in SCD-1 expression was observed and was almost restricted to the basal layer, similar to that in NHS.

3.3. Lipidomic analysis of CERs and FFAs revealed changes in lipid composition upon LXR (de)activation

To determine the effect of LXR (de)activation on SC lipid composition in FTMs, CERs and FFAs were analyzed in details using LC-MS. The amount of extracted lipids from the SC were determined by weighting SC before and after extraction (Supplementary Fig. S3a). The amount of extracted lipids of the various FTMs was similar but significantly lower than NHS. Next, the total amount CERs were quantified by integrating the peaks of their corresponding mass examined (also shown in the ion map Supplementary Fig. S2 for explanations for analyzed CERs and their nomenclature introduced by Motta et al. [21]). The total amount of CERs detected in NHS and FTMs was similar. Next the individual CER (sub)classes were examined. These ceramides were calculated in both absolute amounts (Supplementary Fig. S3) and relative amounts (Fig. 3).

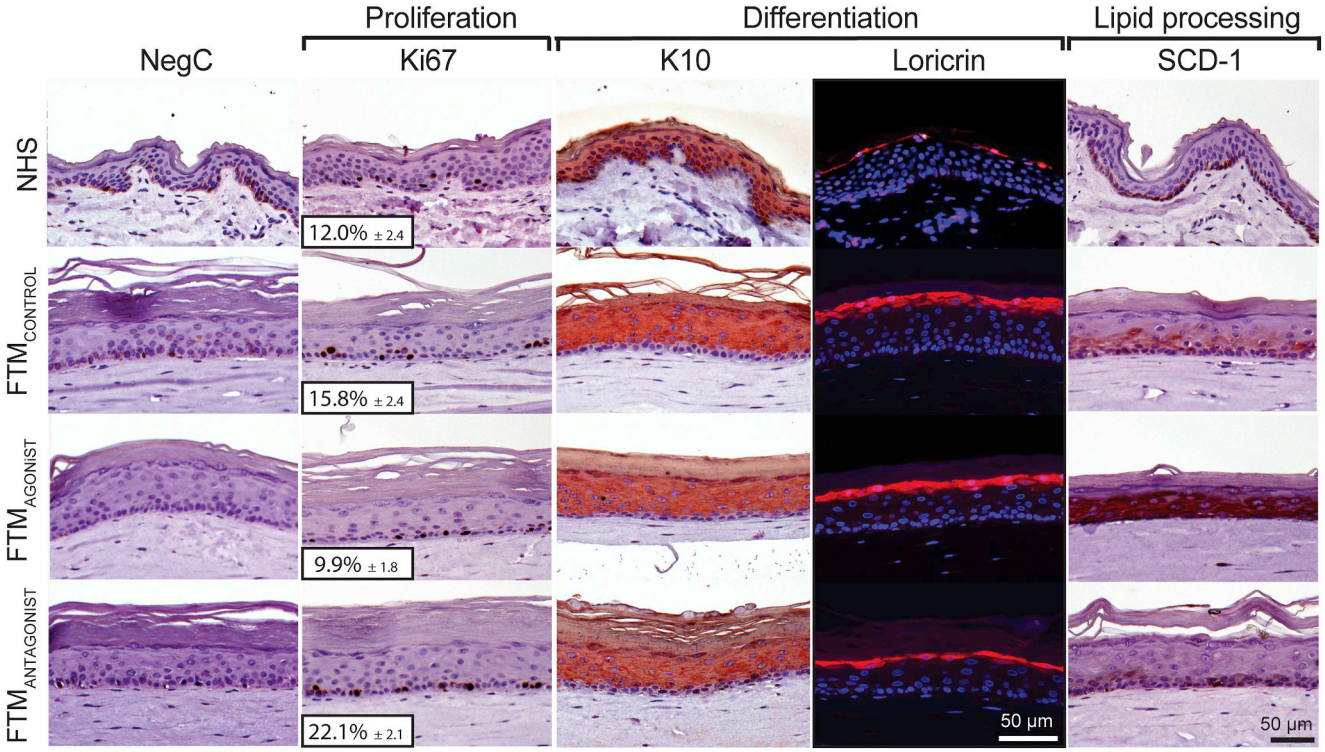

Fig. 2. LXR influences the proliferation and has a strong effect on lipid monounsaturation enzyme SCD-1. Immunohistochemistry/fluorescence staining (from top to bottom): NHS, $FTM_{CONTROL}$, $FTM_{AGONIST}$, and $FTM_{ANTAGONIST}$. The proteins stained (from left to right): negative control (negC), Ki67, K10, loricrin, and SCD-1. Statistics was applied to FTM conditions in an unpaired one-way ANOVA followed by a post Holm-Sidaq test. NHS was compared to the $FTM_{CONTROL}$ with an unpaired *t*-test.

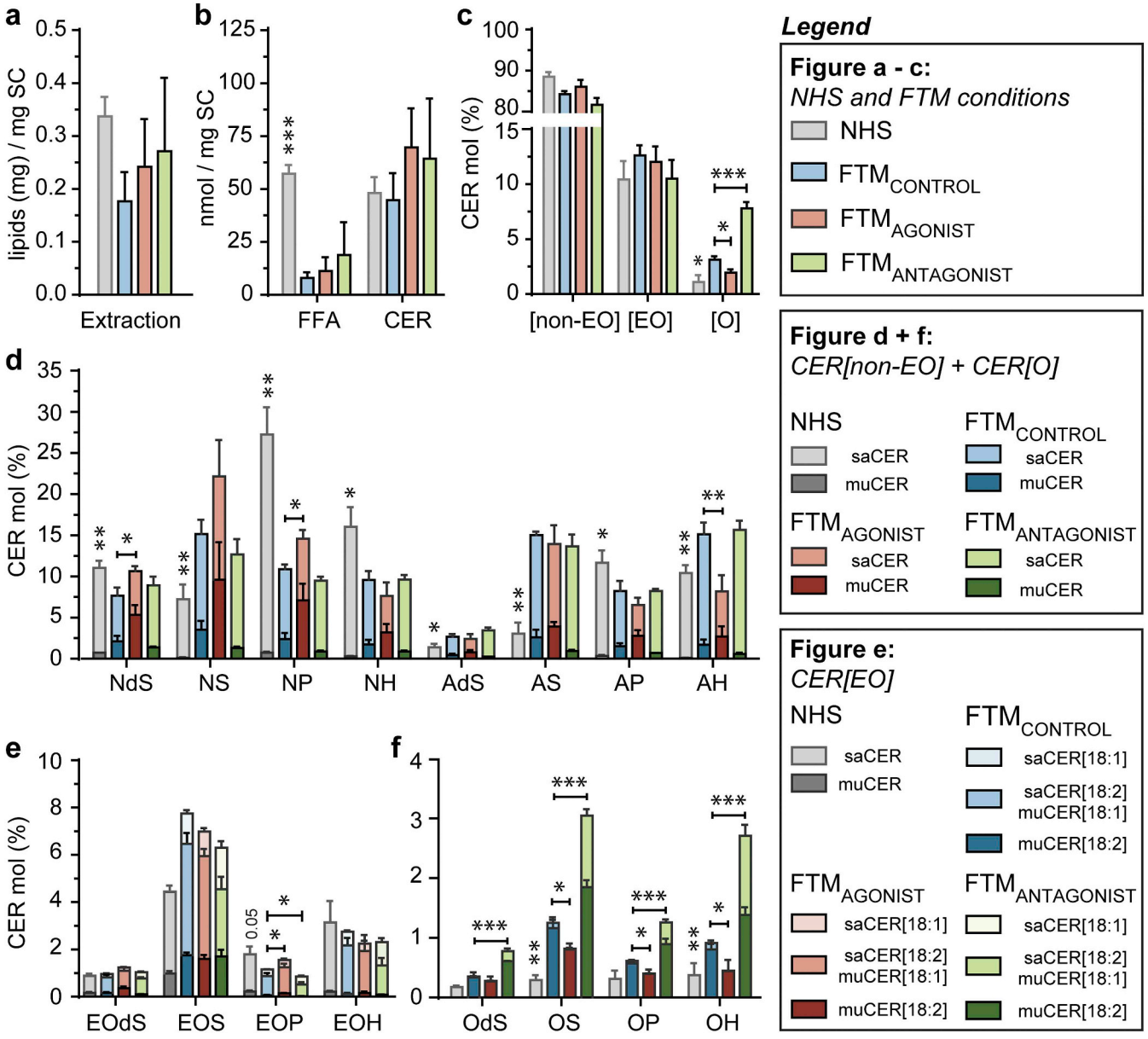

Fig. 3. LXR deactivation did not result in a strong change in the saCER subclass profile, but reduced the fraction of muCERs. (a) Absolute amount of ceramides, (b) distribution of the CER classes, (c), percentage of muCERs[non-EO], (d) CER[non-EO] subclass distribution, (e) CER[EO] subclass distribution and (f) CER[O] subclass distribution. The total level of CER subclasses is set to 100%. Statistics was applied to the FTMs in an unpaired one-way ANOVA followed by a post Holm-Sidaq test. The NHS bar is compared to the $FTM_{CONTROL}$ with an unpaired *t*-test. Data (n = 3) is presented as mean ± SD ($p < 0.05$ = *, $p < 0.01$ = **, $p < 0.001$ = ***).

3.3.1. CER class distribution

When examining the CER[non-EO], CER[EO] and CER[O] classes (Fig. 3b), the relative amount of CER[non-EO] and CER[EO] classes remained similar regardless of LXR (de)activation compared to the $FTM_{CONTROL}$. However, the fraction of CER[O] was increased in $FTM_{ANTAGONIST}$ and reduced in the $FTM_{AGONIST}$ compared to $FTM_{CONTROL}$.

3.3.2. CER[non-EO] subclasses

Next, we determined the percentage of monounsaturation in the total amount of CERs[non-EO] (Fig. 3c). The muCERs were more abundant in the $FTM_{CONTROL}$ compared to NHS. This level was increased even further in $FTM_{AGONIST}$. In contrast to LXR activation, LXR deactivation resulted in a significantly reduced fraction of muCER[non-EO] in the $FTM_{ANTAGONIST}$. To further investigate the effect of LXR (de) activation on the CER subclasses, the amount of saturated (referred to as saCER) and monounsaturated (muCERs) were determined per subclass. In Fig. 3d, the percentages of the total amount of subclass of each CER[non-EO] is provided. In $FTM_{AGONIST}$, the total fraction of the CER[non-EO] subclasses displayed a difference for CER[NdS], CER[NP], and CER[AH] compared to $FTM_{CONTROL}$. However, no change in the CER[non-EO] subclasses was observed in the $FTM_{ANTAGONIST}$ compared to $FTM_{CONTROL}$.

Subsequently, we focus on the percentage of muCER per subclass (individual values with statistics shown in Supplementary Fig. S4a). A reduction in muCERs in the $FTM_{ANTAGONIST}$ was observed for almost all CER[non-EO] subclasses, except for muCER[AdS] and muCER[AH]. This is in contrast to LXR activation, which showed a drastic increase in almost all muCER subclasses compared to $FTM_{CONTROL}$. Finally, we focused on the saCER subclasses (individual values with statistics in Supplementary Fig. S4b) and only minor differences were observed. The level of saCER[NH], saCER[AP], and saCER[AH] was reduced in $FTM_{AGONIST}$. In $FTM_{ANTAGONIST}$, an increase in saCER[NdS] and saCER

[AdS] was observed.

3.3.3. CER[EO] subclasses

In NHS, there is less CER[EO] subclasses present compared to the FTMs. In the CER[EO] subclasses LXR (de)activation only affected the total fraction of CER[EOP] in the FTMs (Fig. 3e) compared to $FTM_{CONTROL}$. However, more differences were observed after a more detailed analysis. In NHS, CER[EO] has an ω-hydroxyl at the acyl chain that is esterified to a linoleic acid (C18:2), this was confirmed by fragmentation (LC-MS/MS). In FTMs, the esterification of this acyl chain can also be linked to oleic acid (C18:1). This CER[EO] will be referred to as CER [EO-18:1] (structure is provided in Supplementary Fig. S2). This led to the detection of four different compositions in each CER[EO] subclass. The saCER[EO-18:2] and the muCER[EO-18:1] could not be distinguished, as they are isobaric compounds with the same retention time. Therefore, the total percentage of these subclasses is provided (Fig. 3e). Although only a minor change in the total fraction of the CER [EO] subclasses was observed, the individual compositions were affected by LXR (de)activation. The muCER[EO-18:2] (statistics provided in Supplementary Fig. S4c) only displayed minor changes in the EOP subclass. However, stronger changes were observed in the main saCER [EO-18:2]/muCER[EO-18:1] (Supplementary Fig. S4d). Here the fraction CER[EOS] was reduced in the $FTM_{ANTAGONIST}$ compared to the $FTM_{CONTROL}$ and the saCER[EO-18:1] fraction (Supplementary Fig. S4e) was significantly increased. This change was most pronounced in saCER [EOS] and saCER[EOH] subclasses compared to $FTM_{CONTROL}$.

3.3.4. CER[O] subclasses

The CER[O] class was detected in low quantities in NHS, but was more abundant in FTMs. The percentage of four CER[O] subclasses (Fig. 3f): CER[OS], CER[OP], and CER[OH] and newly discovered CER [OdS] were influenced by LXR (de)activation [23]. In $FTM_{AGONIST}$, CER [O] subclass fractions were reduced compared to $FTM_{CONTROL}$, whereas $FTM_{ANTAGONIST}$ showed a significant increase in all CER[O] subclasses. Furthermore, in FTMs the CER[O] class mainly consists of muCERs (Supplementary Fig. S4f), but increased amount of saCER[O] (Supplementary Fig. S4g) was also detected in $FTM_{ANTAGONIST}$. CER[O] subclasses are mainly bound as a monolayer to the cornified envelope. Therefore, an increase in CER[O] might be due to a change in the lipid processing to link these lipids to the protein envelope. To obtain evidence for a change in this process the expression of several genes, TGM-1, ALOX-12B, CYP4F22, ALOXE3 and PNPLA-1, contributing to this lipid processing were examined in FTMs. However, gene expression did not differ between tested conditions (Supplementary Fig. S5).

3.3.5. Mean CER carbon chain length

Next to the CER subclass profile, the saturated mean chain length (MCL) of CER subclasses was calculated (Fig. 4a–c). This was calculated from the total number of carbons in each CER (sphingoid base + acyl chain). In $FTM_{AGONIST}$, the MCL was reduced, whereas in $FTM_{ANTAGONIST}$ it was increased and approaching more closely that in NHS. Furthermore, the MCL of CER[EO] and CER[O] classes in $FTM_{ANTAGONIST}$ was even longer than that in NHS.

Another distinction between FTMs and NHS were very short chain length CERs (*m/z* under 600 in the ion map (shown in Supplementary Fig. S2, indicated by a dashed line). In FTMs, a substantial amount of short chain CERs was present with only 34 carbons (referred to as C34-CERs). These C34-CERs were examined as it may play a role in the reduced MCL. The fraction of C34-CERs was higher in $FTM_{CONTROL}$ compared to NHS and increased even more in $FTM_{AGONIST}$ (Fig. 4d). In $FTM_{ANTAGONIST}$, this fraction was reduced significantly approaching more closely the situation in NHS. The absolute quantities of CER[non-EO] as function of chain length (Supplementary Fig. S6a) showed that the reduced MCL in FTMs compared to NHS was attributed to an increase in short chain CER (< C42) rather than the reduction in long chain CERs (≥C42). Although compared to $FTM_{CONTROL}$, $FTM_{ANTAGONIST}$ had not decreased in the amount of short chain CERs, but increased the long chain CERs to an amount mimicking more closely that in NHS. When focusing at percentages CER varying in chain length (Supplementary Fig. S6b), the chain length distribution is even more similar to that in NHS.

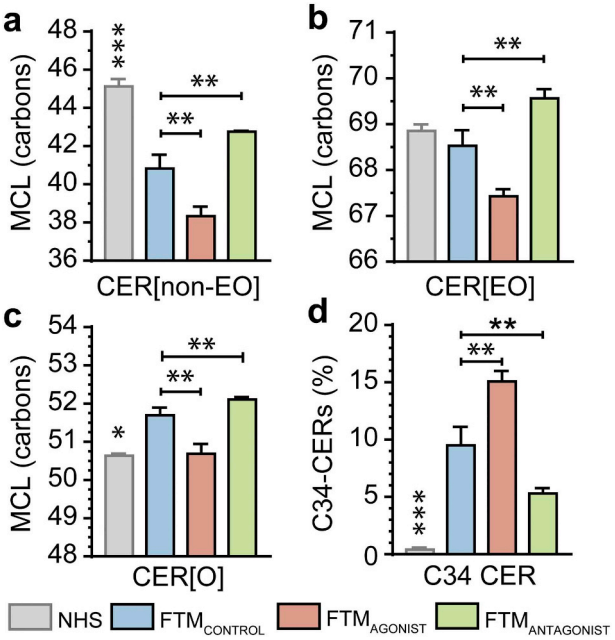

Fig. 4. Differences in MCL of CER classes observed after LXR (de)activation. (a) Saturated mean chain length of the CER[non-EO], (b) CER[EO], (c) CER[O], (d) the percentage of C34-CERs of the total CER[non-EO]. Statistics was applied to the FTMs in an unpaired one-way ANOVA followed by a post Holm-Sidaq test. The NHS bar is compared to the $FTM_{CONTROL}$ with an unpaired *t*-test. Data (n = 3) is presented as mean ± SD ($p < 0.05$ = *, $p < 0.01$ = **, $p < 0.001$ = ***).

3.3.6. FFA composition

In addition to CERs, FFAs were also quantified (absolute values in Supplementary Figs. S7a–b). In the FTMs, there was a significant reduction in the amount of FFA (Fig. 5a) compared to NHS. This reduction was caused by the decrease in the long chain FFA (from C24 to C28). To study the ratios between the FFAs, this data was also plotted in relative amounts (Fig. 5). This included: saturated FFA profile (Fig. 5b), muFFA percentage (Fig. 5c), and MCL (Fig. 5d). Similar trends that were observed in the CERs were also observed in the FFAs. This included an increase in MCL as well as a reduction in the level of muFFAs in $FTM_{ANTAGONIST}$ compared to $FTM_{CONTROL}$.

3.3.7. Cholesterol

LXR is known to influence cholesterol efflux *via* the *ABCA1/ABCG1* transporters. To determine if the level of cholesterol was changed, the cholesterol peak in the ion map was examined. However, no apparent change was observed in the area of cholesterol between the FTMs (Supplementary Fig. S8).

3.4. LXR (de)activation affected the lipid organization in the FTMs, but did not lead to changes in barrier functionality

Alterations in the lipid composition may also lead to changes in the lipid organization. Therefore, both lamellar and lateral organization were investigated. In all FTMs, lipids assembled in a long periodicity phase (LPP) as obtained by X-ray diffraction. From the diffraction peak position, the repeat distance of the LPP was calculated (Fig. 6a). The repeat distance observed in the lipid matrix of $FTM_{CONTROL}$ and $FTM_{ANTAGONIST}$ was similar, but was significantly reduced in $FTM_{AGONIST}$.

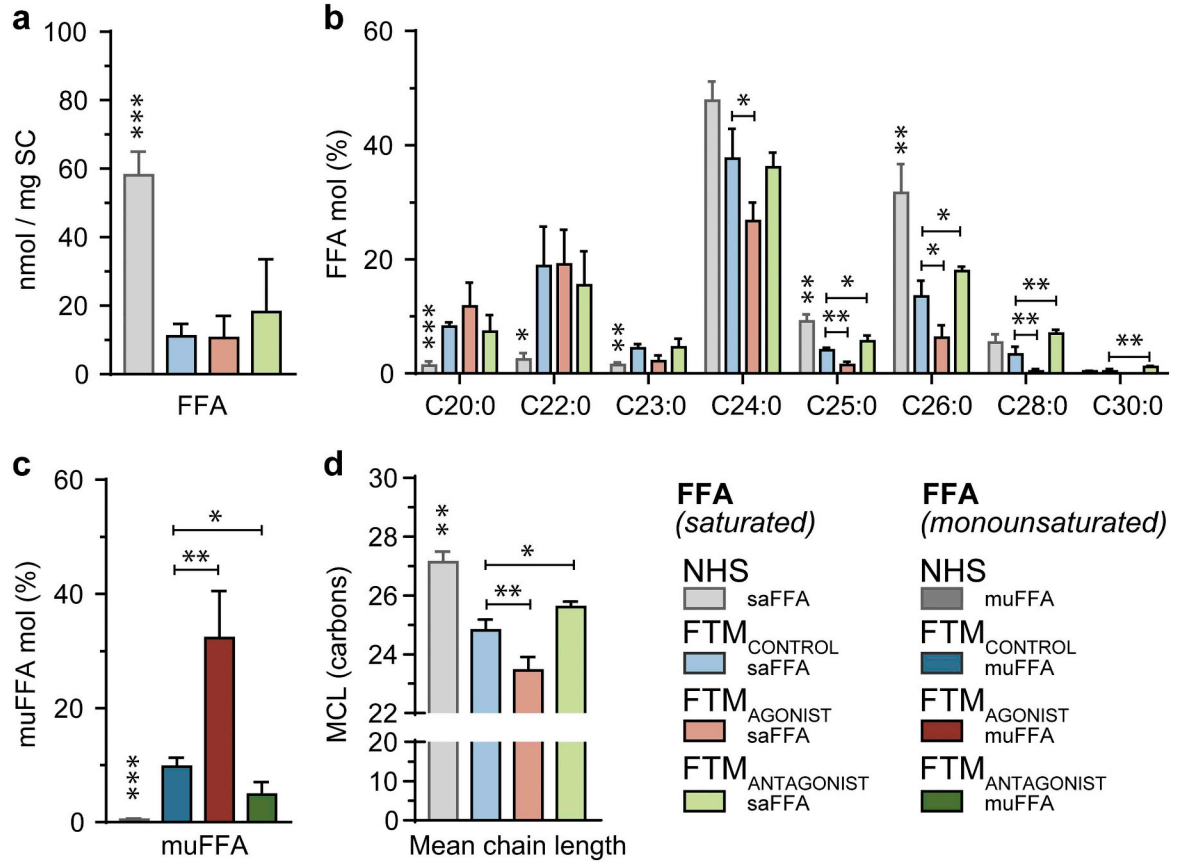

Fig. 5. FFA composition after LXR (de)activation resulted in a change in saturated and monounsaturated FFAs and the mean chain length. (a) Absolute amounts of FFA detected (without C16/C16:1 and C18/C18:1). (b) saFFA chain length distribution was plotted in relative amounts. (c) The percentage of muFFA (C20:1, C22:1, and C24:1) and (d) the saturated MCL. Statistics was applied to FTM conditions in an unpaired one-way ANOVA followed by a post Holm-Sidaq test. NHS was compared to the $FTM_{CONTROL}$ with an unpaired *t*-test. Data is presented as mean ± SD ($p < 0.05$ = *, $p < 0.01$ = **, $p < 0.001$ = ***).

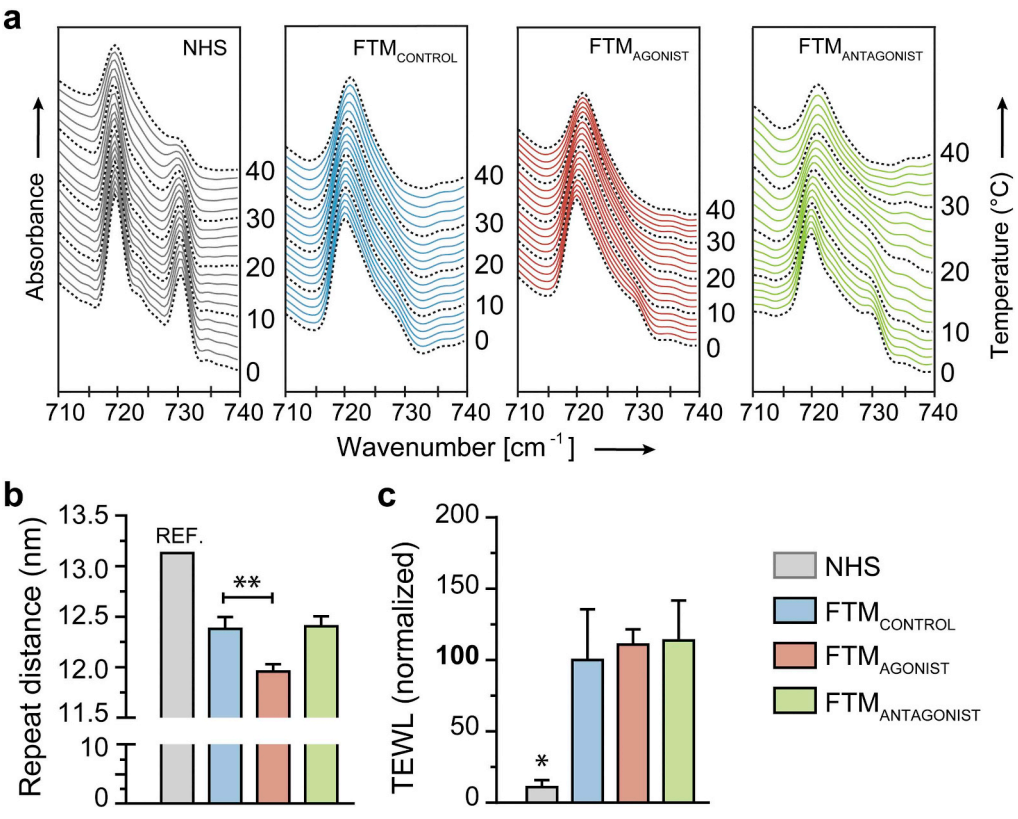

Fig. 6. The effects of LXR (de)activation on the lipid organizations and barrier functionality. NHS and the FTMs are analyzed on: (a) the lateral organization, the plot shows the wavenumbers on the X-axis, corresponding with orthorhombic (doublet at 720 and 730 cm^{-1}) or hexagonal (singlet at 720 cm^{-1}) packing. The samples were measured from 0 to 40 °C, each black dotted line indicates a passage of 10 °C (b) the lipid lamellae repeat distance of the LPP, and (c) the normalized trans epidermal water loss compared to the $FTM_{CONTROL}$. Statistics was applied to the FTMs in an unpaired one-way ANOVA followed by a post Holm-Sidaq test. The NHS bar is compared to the $FTM_{CONTROL}$ with an unpaired *t*-test. Data is presented as mean ± SD ($p < 0.05$ = *, $p < 0.01$ = **).

However, the repeat distance in all FTMs was shorter than in NHS [8].

The lateral packing was monitored by observing the CH_2 rocking vibrations (Fig. 6b) as obtained by Fourier transformed infrared spectroscopy (FTIR). In the FTIR spectrum of NHS, two vibrations were present at 719 and 730 nm^{-1} indicating the presence of lipids assembled in an orthorhombic packing at 0 °C. Upon heating, the 730 nm^{-1} peak weakened and disappeared at 40 °C, indicating a transition to a hexagonal packing. In the FTIR spectra of $FTM_{CONTROL}$ and $FTM_{AGONIST}$, the rocking region displayed a single vibration, indicating only a hexagonal packing. The rocking region of $FTM_{ANTAGONIST}$ showed a shoulder at 730 cm^{-1} at 0 °C, indicating an increased fraction of lipids adopting an orthorhombic packing.

To study whether these changes in lipid organization would affect the barrier, a barrier functionality assay had been performed (Fig. 6c). The trans epidermal water loss (TEWL) was determined for NHS as well as the FTM conditions. Due to the donor variation the models had a different starting TEWL value, therefore the data was normalized to the $FTM_{CONTROL}$ to study the effects for the supplements within the donor. The steady state of the TEWL of NHS (11.0% ± 4.9) was significantly lower compared to the $FTM_{CONTROL}$ (100% ± 35.5%). Surprisingly, the steady state of the $FTM_{AGONIST}$ (110.9% ± 10.6%) and $FTM_{ANTAGONIST}$ (113.8% ± 28.0%) were not significantly altered from the $FTM_{CONTROL}$.

4. Discussion

This study demonstrates that supplementation of GSK2033 in 3D *in vitro* skin models improves the SC lipid profile by a reduction in the quantity of monounsaturated CERs and FFAs combined with a significant increase in the MCL of these lipids more similar to NHS. Supplementation of LXR agonist T0901317 however led to a lipid profile with increased quantity of monounsaturated CERs and FFA followed by a reduction in the MCL more similar to the lipid composition in diseased skin like Netherton syndrome or atopic eczema [13,24]. Supplementation of LXR antagonist GSK2033 had an opposite effect and changed epidermal lipid biosynthesis in a beneficial way as explained below.

1) It reduced SCD-1 expression on gene and protein level and resulted in a CER subclass profile mimicking that of NHS more closely by reducing the fraction of muCER[non-EO] drastically. Although this reduction in monounsaturation was not observed in the muCER[EO-18:2] fraction, the fraction of saCER[EO-18:2]/muCER[EO-18:1] was significantly reduced in the CER[EOS] and CER[EOH] subclasses. The reduction in this fraction and a higher fraction saCER [EO-18:1] may indicate that the latter may be synthetized at the expense of muCER[EO-18:1]. This may indicate that reduction in monounsaturation was also observed in the CER[EO] fraction.
2) It led to a significant increased MCL for all CER classes. This increased MCL was also observed in the FFAs for the $FTM_{ANTAGONIST}$. However, the MCL of both CER and FFA in the $FTM_{AGONIST}$ was significantly reduced. This change in MCL might be attributed to ELOVL1 activity, since ELOVL1 is responsible for the elongation of FFA chains between C18 and C26. According to Ohno et al. [25], reduced activity of ELOVL-1 led to a sphingolipid profile similar to what we observed in the $FTM_{CONTROL}$, containing higher levels of monounsaturation as well as increased shorter chain lipids [26,27]. In addition, activity of ELOVL1 is reduced by the presence of monounsaturated FFAs such as C18:1 and C20:1 [28]. This could explain why no changes were observed on ELOVL1 gene level, but changes were observed in the lipid composition in the FTMs as well as compared to NHS.
3) It resulted in a small increase in the fraction of lipids forming an orthorhombic lateral packing at temperatures below 22 °C. This improved lipid organization may be attributed to the reduction in muCERs and muFFAs and an increase in the chain lengths of CERs and FFAs. Both changes are known to enhance the formation of an orthorhombic lateral packing [12,13]. No differences were observed in the barrier functionality between the $FTM_{AGONIST}$ and $FTM_{ANTAGONIST}$ at 25 °C, most probably due to the absence of an improved lipid organization at this temperature. This does indicate that there are other important factors still required to form a proper barrier at 25 °C. One of these factors might be the low amount of FFAs in FTMs. Studies have shown that FFAs are crucial for the formation of the orthorhombic packing [29,30]. A higher level of FFA in FTMs may further increase the fraction of lipids forming an orthorhombic packing. To achieve this is of interest to study in the future.

However, an unexpected effect of LXR deactivation was an increase in the CER[O] fraction. In NHS, CER[O] are present in low amounts in the lipid matrix, but are also found chemically linked to the cornified envelope (bound CER[O]). In this process, during various synthetic steps, glucosylCER[EO] (also the precursors of CER[EO]) are converted into bound CER[O]. This is performed by various enzymes. *ALOX-12B* and *ALOX-E3* are required for the LOX-mediated oxygenation of CER [EO] [31,32], while *TGM-1* is important for binding to the cornified envelope [33–35]. The enzymes *CYP4F22* and *PNPLA-1* which are involved in the ω-hydroxy synthesis play also an important role [35–37]. However, no differences in gene expression of these enzymes were observed between FTMs. A detailed quantification of the bound lipids may provide additional insight regarding this part, but this was not the scope of the present study.

Another aspect of LXR is the influence on the epidermal homeostasis. LXR is known to be a pro-differentiation Results in mice indicate the stimulation of the epidermal differentiation as well as the lipid synthesis [39–40]. In our FTMs, LXR (de)activation led to similar effects whereas the LXR antagonist increased the proliferation and slightly decreased loricrin expression but the lipid quantification did not reveal an increase in lipid synthesis. In addition, LXR activation has a potent anti-inflammatory effect by reducing the TNF-α and interleukin-1α [41], which is regarded as beneficial for barrier repair. However, in our FTMs we did not investigate cytokine production as no immune cells are incorporated in the model.

When comparing the effect of LXR (de)activation on the lipid biosynthesis in various models, similarities are observed. In keratinocyte monolayers, supplementation of T0901317 (1 μM) increased the lipid synthesis genes SREBP1, FAS, and SCD1 [42]. In addition, cholesterol and phospholipid transporters such as ABCA1, ABCG1, and ABCA12 were increased as well. These effects were also observed in murine models, in which LXR activation is associated with barrier repair by stimulating lipid synthesis (SREBP-1c, FAS, SCD-1) [43,44], lipid transport (ABCA1, and ABCG1) and increasing lamellar body formation (ABCA12) [38,45].

However, murine skin predominantly expresses LXR-β, whereas human skin also expresses LXR-α [46–48]. In LXR-α knockout mice, it was observed that liver *SREBP*-1, *FAS*, and *SCD-1 genes* were reduced, indicating that LXR-α has a lipogenic role [49].

Recently a clinical study has been published in which an LXR agonist was used to assess safety and tolerability as well as cellular and molecular changes when applied to the skin [50]. In that study, the lipogenic genes were increased. However, neither the barrier lipids were quantified nor the lipid composition was determined. The results of this study suggest that for improved lipid properties rather an LXR antagonist, than an agonist should be used to improve the skin lipid properties of these patients. In the present study, LXR (de)activation led to a trend in the increase of lipogenic genes *FAS*, *ACC1*, and *SREBP1*, but did not result in significant changes. This is consistent with similar absolute amounts of CERs and FFA detected in the SC of FTMs regardless of LXR (de)activation. The strongest change in the FTMs after LXR (de)activation was observed on the gene and protein expression of SCD-1. This might be explained by the fact that *SCD-1* has a response element for both *SREBP1* and *LXR* [16].

Besides the complexity of the *in vitro* and *in vivo* correlations, in literature it has been reported that T091317 and GSK2033 can activate other nuclear receptors, such as the pregane-X-receptor (PXR), farnesoid-X-receptor (FXR), vitamin D receptor (VDR) [43,51–54]. However, recently it was reported that specific VDR targeting by supplementation of $1,25(OH)_2D_3$ did not lead to changes in the lipid composition of FTMs [55]. The role of other receptors such as PXR were investigated by supplementation of LXR agonist T0901317 and the specific LXR agonist GW3965 [43]. When comparing the lipogenic effects of LXR agonist T0901317 and the specific LXR agonist GW3965, the effects on gene level were similar for ABCA1, SREBP-1c, FAS, and SCD-1 *in vitro* in HepG2 cells. Whereas in murines, the lipogenic effects of T091317 resulted in a stronger activation of SREBP-1c, SCD-1, and FAS. This indicates that the increase in these genes cannot be ascribed to LXR (de) activation alone. Although interesting to determine the effect of the other receptors, the scope of this study was to determine whether it is possible to improve the composition of the barrier lipids by the use of GSK2033, which is indeed the case.

To conclude, this work demonstrates the role of the LXR supplements T0901317 and GSK2033 on the epidermal homeostasis and lipid synthesis in our full thickness skin model. LXR deactivation resulted in a reduced fraction of monounsaturated lipids and an increase in chain length of CERs and FFAs. This improved the composition and lipid organization, but was not enough to change the functional skin barrier. This improvement will be one of the steps in the generation of HSEs which represent the barrier of NHS more closely.

Declaration of competing interest

The authors declare that they have no known competing financial interests or personal relationships that could have appeared to influence the work reported in this paper.

Transparency document

The Transparency document associated this article can be found, in online version.

CRediT authorship contribution statement

Richard W.J. Helder: Conceptualization, Methodology, Resources, Investigation, Formal analysis, Visualization, Writing - original draft, Writing - review & editing. **Walter A. Boiten:** Software, Formal analysis. **Rianne van Dijk:** Methodology, Formal analysis. **Gerrit S. Gooris:** Software, Formal analysis. **Abdoelwaheb El Ghalbzouri:** Conceptualization, Methodology, Supervision, Project administration, Funding acquisition, Writing - review & editing. **Joke A. Bouwstra:** Conceptualization, Methodology, Supervision, Project administration, Funding acquisition, Writing - review & editing.

Acknowledgements

This research was supported by the Dutch Technology Foundation STW (Grant 13151) and is part of the Netherlands Organization for Scientific Research (NWO). We also would like to thank the DUBBLE beam line BM26 staff at the European synchrotron radiation facility (Grenoble, France) for their support and the company Evonik for their supply of ceramides.

Appendix A. Supplementary data

Supplementary data to this article can be found online at https://doi.org/10.1016/j.bbalip.2019.158546.

References

[1] H. Niehues, et al., 3D skin models for 3R research: the potential of 3D reconstructed skin models to study skin barrier function, Exp Dermatol. 27 (5) (2018) 501–511.
[2] A. El Ghalbzouri, et al., Leiden reconstructed human epidermal model as a tool for the evaluation of the skin corrosion and irritation potential according to the ECVAM guidelines, Toxicol. in Vitro 22 (5) (2008) 1311–1320.
[3] V.S. Thakoersing, et al., Unraveling barrier properties of three different in-house human skin equivalents, Tissue Eng Part C Methods 18 (1) (2012) 1–11.
[4] Y. Masukawa, et al., Comprehensive quantification of ceramide species in human stratum corneum, J. Lipid Res. 50 (8) (2009) 1708–1719.
[5] M. Rabionet, K. Gorgas, R. Sandhoff, Ceramide synthesis in the epidermis, Biochim. Biophys. Acta 1841 (3) (2014) 422–434.
[6] J. van Smeden, et al., LC/MS analysis of stratum corneum lipids: ceramide profiling and discovery, J. Lipid Res. 52 (6) (2011) 1211–1221.
[7] J. t' Kindt, et al., Profiling and characterizing skin ceramides using reversed-phase liquid chromatography-quadrupole time-of-flight mass spectrometry, Anal. Chem. 84 (1) (2012) 403–411.
[8] J.A. Bouwstra, et al., Structural investigations of human stratum corneum by small-angle X-ray scattering, J Invest Dermatol. Dec(6) (1991) 1005–1012.
[9] M. Ponec, et al., The formation of competent barrier lipids in reconstructed human epidermis requires the presence of vitamin C, J Invest Dermatol. 109 (3) (1997) 348–355.
[10] S.T. Boyce, M.L. Williams, Lipid supplemented medium induces lamellar bodies and precursors of barrier lipids in cultured analogues of human skin, J Invest Dermatol. 101 (2) (1993) 180–184.
[11] V.S. Thakoersing, et al., Increased presence of monounsaturated fatty acids in the stratum corneum of human skin equivalents, J. Investig. Dermatol. 133 (1) (2013) 59–67.
[12] E.H. Mojumdar, et al., Monounsaturated fatty acids reduce the barrier of stratum corneum lipid membranes by enhancing the formation of a hexagonal lateral packing, Langmuir. 30 (22) (2014) 6534–6543.
[13] J. van Smeden, et al., The importance of free fatty acid chain length for the skin barrier function in atopic eczema patients, Exp. Dermatol. 23 (1) (2014) 45–52.
[14] J. Ishikawa, et al., Changes in the ceramide profile of atopic dermatitis patients, J Invest Dermatol. 130 (10) (2010) 2511–2514.
[15] C.M. Paton, J.M. Ntambi, Biochemical and physiological function of stearoyl-CoA desaturase, Am. J. Physiol. Endocrinol. Metab. 297 (1) (2009) E28–E37.
[16] J.R. Schultz, et al., Role of LXRs in control of lipogenesis, Genes Dev. 14 (2000) 2831–2838.
[17] V.S. Thakoersing, et al., Modulation of stratum corneum lipid composition and organization of human skin equivalents by specific medium supplements, Exp. Dermatol. 24 (9) (2015) 669–674.
[18] V. van Drongelen, et al., Barrier properties of an N/TERT-based human skin equivalent, Tissue Eng Part A. 20 (21 – 22) (2014) 3041–3049.
[19] E.M. Haisma, et al., Inflammatory and antimicrobial responses to methicillin-resistant Staphylococcus aureus in an in vitro wound infection model, PLoS One 8 (12) (2013) 11.
[20] W.A. Boiten, et al., Quantitative analysis of ceramides using a novel lipidomics approach with three dimensional response modelling, Biochim. Biophys. Acta 1861 (11) (2016) 1652–1661.
[21] S. Motta, et al., Ceramide composition of the psoriatic scale, Biochim. Biophys. Acta 1182 (2) (1993) 147–151.
[22] M. Janssens, et al., Increase in short-chain ceramides correlates with an altered lipid organization and decreased barrier function in atopic eczema patients, J. Lipid Res. 53 (12) (2012) 2755–2766.
[23] W.A. Boiten, et al., Selectivity in cornified envelop binding of ceramides in human skin and the role of LXR inactivation on ceramide binding, Biochim. Biophys. Acta Mol. Cell Biol. Lipids 1864 (9) (2019) 1206–1213.
[24] J. van Smeden, et al., Intercellular skin barrier lipid composition and organization in Netherton syndrome patients, J Invest Dermatol. 134 (5) (2014) 1238–1245.
[25] Y. Ohno, et al., ELOVL1 production of C24 acyl-CoAs is linked to C24 sphingolipid synthesis, PNAS 107 (43) (2010) 18439–18444.
[26] T. Sassa, A. Kihara, Metabolism of very long-chain fatty acids: genes and pathophysiology, Biomol Ther (Seoul) 22 (2) (2014) 83–92.
[27] T. Sassa, et al., Impaired epidermal permeability barrier in mice lacking elovl1, the gene responsible for very-long-chain fatty acid production, Mol. Cell. Biol. 33 (14) (2013) 2787–2796.
[28] T. Sassa, et al., Lorenzo's oil inhibits ELOVL1 and lowers the level of sphingomyelin with a saturated very long-chain fatty acid, J. Lipid Res. 55 (3) (2014) 524–530.
[29] G.S. Gooris, J.A. Bouwstra, Infrared spectroscopic study of stratum corneum model membranes prepared from human ceramides, cholesterol, and fatty acids, Biophys. J. 92 (8) (2007) 2785–2795.
[30] J.A. Bouwstra, et al., Phase behavior of lipid mixtures based on human ceramides: coexistence of crystalline and liquid phases, J. Lipid Res. 42 (11) (2001) 1759–1770.
[31] Y. Zheng, et al., Lipoxygenases mediate the effect of essential fatty acid in skin barrier formation: a proposed role in releasing omega-hydroxyceramide for construction of the corneocyte lipid envelope, J. Biol. Chem. 286 (27) (2011) 24046–24056.
[32] P. Krieg, et al., Aloxe3 knockout mice reveal a function of epidermal lipoxygenase-3 as hepoxilin synthase and its pivotal role in barrier formation, J Invest Dermatol. 133 (1) (2013) 172–180.
[33] M. Matsuki, et al., Defective stratum corneum and early neonatal death in mice lacking the gene for transglutaminase 1 (keratinocyte transglutaminase), Proc. Natl.

Acad. Sci. U. S. A. 95 (3) (1998) 1044–1049.
[34] N. Nakagawa, et al., Knocking-in the R142C mutation in transglutaminase 1 disrupts the stratum corneum barrier and postnatal survival of mice, J. Dermatol. Sci. 65 (3) (2012) 196–206.
[35] P. Krieg, G. Fürstenberger, The role of lipoxygenases in epidermis, Biochim. Biophys. Acta 1841 (2014) 390–400.
[36] Y. Ohno, et al., Essential role of the cytochrome P450 CYP4F22 in the production of acylceramide, the key lipid for skin permeability barrier formation, Proc. Natl. Acad. Sci. U. S. A. 112 (25) (2015) 6.
[37] S. Grond, et al., PNPLA1 deficiency in mice and humans leads to a defect in the synthesis of omega-O-acylceramides, J Invest Dermatol. 137 (2) (2017) 394–402.
[38] M.Q. Man, et al., Basis for improved permeability barrier homeostasis induced by PPAR and LXR activators: liposensors stimulate lipid synthesis, lamellar body secretion, and post-secretory lipid processing, J Invest Dermatol. 126 (2) (2006) 386–392.
[39] M. Schmuth, et al., Peroxisome proliferator-activated receptors and liver X receptors in epidermal biology, J. Lipid Res. 49 (2008) 11.
[40] M. Schmuth, et al., Role of PPAR, LXR, and PXR in epidermal homeostasis and inflammation, Biochim. Biophys. Acta 1 (1841) (2014) 463–473.
[41] A.J. Fowler, et al., Liver X receptor activators display anti-inflammatory activity in irritant and allergic contact dermatitis models: liver-X-receptor-specific inhibition of inflammation and primary cytokine production, J. Invest. Dermatol. 120 (2003) 246–255.
[42] K.C. Chang, et al., Liver X receptor is a therapeutic target for photoaging and chronological skin aging, Mol. Endocrinol. 22 (11) (2008) 2407–2419.
[43] N. Mitro, et al., T0901317 is a potent PXR ligand: implications for the biology ascribed to LXR, FEBS Lett. 581 (9) (2007) 1721–1726.
[44] S.B. Joseph, et al., Direct and indirect mechanisms for regulation of fatty acid synthase gene expression by liver X receptors, J. Biol. Chem. 277 (13) (2002) 11019–11025.
[45] K. Hanley, et al., Activators of the nuclear hormone receptors PPARalpha and FXR accelerate the development of the fetal epidermal permeability barrier, J. Clin. Invest. 100 (3) (1997) 705–712.
[46] L.E. Russell, et al., Characterization of liver X receptor expression and function in human skin and the pilosebaceous unit, Exp. Dermatol. 16 (10) (2007) 844–852.
[47] P.A. Edwards, M.A. Kennedy, P.A. Mak, LXRs; oxysterol-activated nuclear receptors that regulate genes controlling lipid homeostasis, Vasc. Pharmacol. 38 (4) (2002) 249–256.
[48] E.G. Lund, et al., Different roles of liver X receptor a and b in lipid metabolism: effects of an a-selective and a dual agonist in mice deficient in each subtype, Biochem. Pharmacol. 71 (4) (2006) 453–463.
[49] E.M. Quinet, et al., Liver X receptor (LXR) - regulation in LXR - deficient mice: implications for therapeutic targeting, Mol. Pharmacol. 70 (4) (2006) 1340–1349.
[50] T. Czarnowicki, et al., Effect of short-term liver X receptor activation on epidermal barrier features in mild to moderate atopic dermatitis: a randomized controlled trial, Ann. Allergy Asthma Immunol. 120 (6) (2018) 631–640.
[51] K.A. Houck, et al., T0901317 is a dual LXR/FXR agonist, Mol. Genet. Metab. 83 (1–2) (2004) 184–187.
[52] C. Handschin, U.A. Meyer, Regulatory network of lipid-sensing nuclear receptors: roles for CAR, PXR, LXR, and FXR, Biochemistry and Biophysics 433 (2) (2005) 387–396.
[53] K. Griffett, T.P. Burris, Promiscuous activity of the LXR antagonist GSK2033 in a mouse model of fatty liver disease, Biochem. Biophys. Res. Commun. 479 (3) (2016) 424–428.
[54] Y. Lim, J. Huang, Interplay of pregnane X receptor with other nuclear receptors on gene regulation, Drug Metabolism and Pharmacokinetics. 23 (1) (2008) 14–21.
[55] A. Mieremet, et al., Shedding light on the effects of 1,25-dihydroxyvitamin D3 on epidermal lipid barrier formation in three-dimensional human skin equivalents, J. Steroid Biochem. Mol. Biol. 189 (2019) 19–27.